Ferreiro-Córdova, C., Royall, C. P., & Van Duijneveldt, J. S. (2020). Anisotropic viscoelastic phase separation in polydisperse hard rods: non-sticky gelation. *Proceedings of the National Academy of Sciences of the United States of America*, *117*(7), 3415-3420. https://doi.org/10.1073/pnas.1909357117

Anisotropic viscoelastic phase separation in polydisperse hard rods: non-sticky gelation

Claudia Ferreiro-Córdova[a,b,d], **C. Patrick Royall**[a,b,c,1], **and Jeroen S. van Duijneveldt**[a]

[a]School of Chemistry, Cantock's Close, University of Bristol, BS8 1TS, UK.; [b]Centre for Nanoscience and Quantum Information, Tyndall Avenue, Bristol BS8 1FD, UK; [c]H.H. Wills Physics Laboratory, Tyndall Ave., Bristol, BS8 1TL, UK; [d]Laboratoire de Physique des Solides, CNRS, Université Paris-Sud, Université Paris-Saclay, 91405 Orsay, France.

This manuscript was compiled on December 23, 2019

Spinodal demixing into two phases having very different viscosities leads to viscoelastic networks, i.e. gels, usually as a result of attractive particle interactions. Here, however, we demonstrate demixing in a colloidal system of polydisperse rod-like clay particles that is driven by particle repulsions instead. One of the phases is a nematic liquid crystal with a highly anisotropic viscosity, allowing flow along the director but suppressing it in other directions. This phase coexists with a dilute isotropic phase. Real-space analysis and molecular dynamics simulations both reveal a long-lived network structure that is locally anisotropic yet macroscopically isotropic. We show that our system exhibits the characteristics of colloidal gelation and conclude that it represents a new class of material, *non-sticky* gels.

Liquid crystals | Gels | Colloidal rods

Gelation, the emergence of a network of arrested material, is among the most striking everyday features of soft condensed matter (1) and is an example of viscoelastic phase separation where a contrast in viscosity between the demixed phases leads to the formation of a long-lived network (2). Gels can be soft (and biological) materials such as proteins (3), clays (4), foods (5), hydrogels (6) and tissues (7). In addition, a more diverse range of materials including granular matter (8), phase-demixing oxides (9) and metallic glass formers (10) also exhibit gelation.

Despite its widespread occurrence, a complete understanding of gelation remains a challenge (1). Two properties unify particulate gels produced to date. Firstly, the constituent particles experience a significant *attraction* to one another (which may be effective, induced for example by depletion effects from added polymer (11)), resulting in phase separation that arrests before completion. Secondly, with some exceptions, such as local crystallisation (12), both phases are *isotropic*. The interparticle attraction is closely related to the phase behaviour. In gelation, spinodal decomposition (immediate demixing) leads to a "colloidal liquid" phase which is of sufficient volume fraction that its high viscosity results in a long-lived network in which full demixing is suppressed (1, 2, 13, 14). Thus colloidal gels exhibit *dynamical contrast* between the phases formed through spinodal decomposition (15).

Here we depart from this paradigm of gelation driven by attraction between particles: we consider a system of polydisperse colloidal rods without significant attractions. Nevertheless in such a system, spinodal decomposition occurs from a thermodynamically unstable isotropic fluid to an isotropic fluid in coexistence with a nematic liquid crystal (16–18).

While the phase behavior and spinodal mechanism of demixing suggests that gelation may be found, it is important to consider the dynamics: why should the phase separation in our system arrest such that a gel forms? Now the nematic phase exhibits an *anisotropic viscosity*. Although the viscosity along the director is comparable to that in the isotropic phase, perpendicular to the director, the viscosity is much higher for our polydisperse system. For suitable compositions, we furthermore expect percolation of the nematic phase. We shall show that the rods align parallel to the "arms" of the gel, and thus while there may be flow along the arms, perpendicular flow is very strongly suppressed. We thus argue that polydisperse rods in which attraction is not important feature many of the properties required for spinodal gelation. This concept of gels formed by nematic-isotropic spinodal decomposition is shown in Fig. 1.

We identify four criteria of spinodal gelation (2). *(i)* The system must undergo spinodal decomposition; *(ii)* There must be *dynamic asymmetry* between the phases (that is to say, one phase is substantially more viscous that the other); *(iii)* The more viscous phase must percolate (19); *(iv)* The non-equilibrium nature of the gel leads to aging, in particular coarsening.

To realise such materials, we combine real space analysis of a colloidal model system of polydisperse hard rods with computer simulation to demonstrate the character of *non-sticky gelation*. Our sepiolite colloidal rods exhibit two features which are important here. Firstly, any attractions are small, as the phase diagram is consistent with that of polydisperse hard rods (20) and, as we shall show, computer simulations without any attractions exhibit the same behaviour. This means that any gelation behaviour we find is not attributed to attractions or even effective attractions such as those found in colloid-polymer

Significance Statement

Networks of mesoscopic colloidal particles, gels, are an everyday material, from cosmetics to foods. Yet our understanding of colloidal gels lags far behind their utility: gels are out-of-equilibrium, so their properties change over time, often with significant consequences, such as failure of the material. However until now, we were confident of one thing: to aggregate into a network, the colloidal particles need to attract one another. Here we show that in fact colloids can form a network without significant attractions. This is surprising because particles without an attraction usually distribute themselves throughout space, rather than forming a network of particle-rich and poor regions. Our work opens the way to new materials – "non-sticky gels" – and a deeper understanding of this perplexing state of matter.

All authors designed the research and wrote the paper. CFC carried out the experiments, simulations and data analysis.

The authors declare no conflict of interest.

[1]To whom correspondence should be addressed. E-mail: Paddy.Royall@bristol.ac.uk

mixtures (11). Secondly, the rods are rather polydisperse (with an effective aspect ratio $\langle L'/D' \rangle = 24.6 \pm 9.5$) leading to a large gap in volume fraction between isotropic and nematic phases at phase coexistence (Fig 2). While this coexistence gap might shrink on long timescales due to segregation of the rods (21), this is suppressed by the slow dynamics of the nematic phase and no evidence of segregation is seen on the experimental timescale.

The fact that the rods undergo spinodal decomposition satisfies criterion (*i*), and the large gap in volume fraction between isotropic and nematic phases at coexistence suggests that the latter may exhibit slow dynamics, satisfying criterion (*ii*). Criterion (*iii*), of percolation, also follows from spinodal decomposition, likewise criterion (*iv*), of aging. It is thus possible that the criteria identified for spinodal gelation are met by this system of rods, and this we go on to show.

1. Experimental and simulation methodology

Experimental system — . The isotropic-nematic phase separation of colloidal suspensions of fluorescently labeled sepiolite clay particles was studied using confocal imaging of samples with concentrations in the coexistence range. The phase diagram of our system was determined before confocal analysis, and from this we extracted the range of concentrations of interest. Here we use the *effective* bulk rod volume fraction ϕ as a measure of the concentration, which is determined from the number density of rods and the mean rod volume. Rods are taken to be cylinders of length equal to that measured with TEM plus 2δ, and diameter equal to the width measured plus 2δ. Here $\delta = 4$ nm, the lengthscale of steric stabilization. The number density is determined from the mass fraction and rod mass density.

Confocal images of the system were obtained with a Leica SP5 confocal microscope using a white light laser emitting at 500 nm. Borosilicate glass capillaries with cross sections of 1×0.1 mm were filled with rod suspensions at effective volume fractions of $\phi = 0.021, 0.026, 0.031, 0.043, 0.054, 0.066$ and glued to microscope slides with epoxy. The samples were stirred using a vortex mixer for one minute before filling the capillaries. Our analysis focuses on the time evolution of the phase separation, for which we have defined $t = 0$ as the moment when the stirring stops. We presume that the vortex mixing leaves the system in an isotropic state, and that $t = 0$ is the start of the demixing.

Computer Simulation — . We modelled the experimental system using rods with a steep repulsive interaction. We use molecular dynamics and neglect the effect of solvent-mediated hydrodynamic interactions. Significant though these are (22), here we choose to focus our computational resources on simulating as large a system size as possible, so that the length– and time–scales may be comparable to the experiments. Our systems consisted of up to 180,000 rods with polydispersity only in length. The length distribution of our model rods is described by a Gaussian with an average rod length of $L = 24.48\sigma \pm 9.06\sigma$. Three different global volume fractions are explored here: $\phi = 0.012$ (isotropic), $\phi = 0.145$ (coexistence) and $\phi = 0.357$ (nematic). For $\phi = 0.145$ we found a phase coexistence with around 40% of the rods in a highly aligned nematic phase. The snapshots shown correspond to a system of 180,000 rods with a volume fraction $\phi = 0.140$ which corresponds to phase coexistence. Further details can be found in Methods and Supplementary Information (SI).

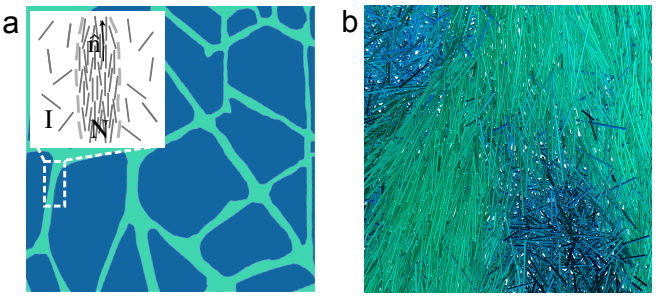

Fig. 1. Schematic illustration of anisotropic viscoelastic phase separation. Spinodal decomposition leads to a bicontinuous network of isotropic (I) and nematic (N). (a) Inset shows that rods align parallel to the director, indicated as $\hat{\mathbf{n}}$. We expect that the viscosity parallel to the director is low enough to permit flow, while perpendicular flow is strongly suppressed. (b) Snapshot of a thin slice of a simulation box of rods at $\phi = 0.140$. Colours indicate the local order parameter S_i of each rod i (see SI), and range from dark blue (isotropic) to bright green (nematic).

2. Non-sticky gels of polydisperse rods

Our presentation of results is as follows. First we consider the phase behaviour. While the isotropic-nematic transition of long rod-shaped particles has been known since the pioneering work of Onsager (23), our results show the importance of polydispersity in broadening the coexistence gap of the isotropic-nematic transition, with a nematic phase whose density is around nine times that of the isotropic phase (20). Note that the viscosity of the nematic phase varies markedly with respect to the mean rod orientation (24, 25), which has significant consequences for the behaviour of the networks we obtain.

Secondly, we consider spinodal decomposition, which we demonstrate leads to a percolating network of nematic phase. We then determine the dynamical asymmetry between the isotropic and nematic phases and find the latter to be very much more viscous than the former, for flow perpendicular to the director. Finally we consider coarsening of the network. We find behaviour broadly similar to that known for spinodal gels formed of spheres (13, 15, 26), but we emphasise that the gels we obtain should exhibit flow along channels comprised by the nematic phase but that perpendicular flow should be suppressed, as our simulations show that rods align parallel to the nematic domains (Fig. 1).

A. Phase Behaviour. We present the phase diagram of our system in Fig. 2. Here we consider the fraction of nematic phase $f_{\rm nem}$ as a function of (effective) volume fraction ϕ obtained from bulk observations of phase coexistence (see Methods). The key point is that the isotropic-nematic phase coexistence is very substantially broadened due to polydispersity, as indicated in the yellow shaded region in Fig. 2. Such broadening due to polydispersity is in *quantitative agreement* with theoretical predictions for hard rods (21, 27). The (effective) volume fractions of the isotropic and the nematic phase in the coexistence were calculated by fitting the experimental data in Fig. 2 to a straight line. The ratio of the volume fractions at coexistence for our polydisperse system is $\phi^{\rm coex}_{\rm nem}/\phi^{\rm coex}_{\rm iso} = 0.215/0.024 = 9.00$, while that for a monodisperse system of very similar aspect ratio $L/D = 25$, is just $\phi^{\rm coex}_{\rm nem}/\phi^{\rm coex}_{\rm iso} = 0.157/0.127 = 1.22$ (28). Thus polydispersity

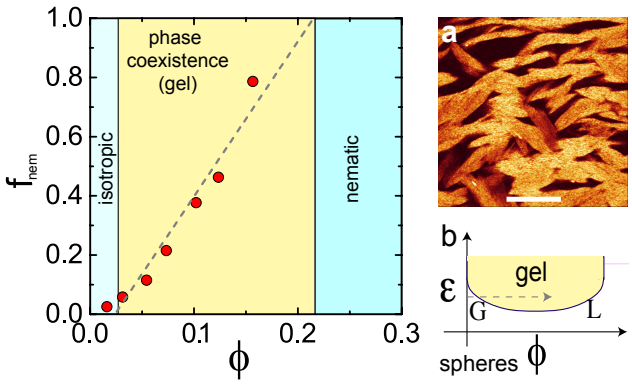

Fig. 2. Gelation via isotropic-nematic spinodal decomposition in polydisperse hard rods. The fraction of the nematic phase $f_{\rm nem}$ is plotted as a function of global volume fraction ϕ. Phase coexistence occurs between $\phi_{\rm iso}^{\rm coex} = 0.024$ and $\phi_{\rm nem}^{\rm coex} = 0.215$ for the isotropic and nematic phases respectively and it is in this region of the phase diagram that gelation occurs (yellow shaded region). Red data points are experimental state points where we have determined $f_{\rm nem}$. (a) Confocal image of nematic gel formed in a sample at an initial bulk volume fraction $\phi = 0.043$ for a demixing time lapse of $t = 2$h. Bright regions indicate the nematic phase. Scale bar represents 4 μm. (b) Gelation in a typical system of spheres with attraction. Shown is the phase diagram in the attraction strength ε—volume fraction ϕ plane. Here gelation also occurs via spinodal decomposition, but this requires sufficient attraction for spinodal decomposition to a colloidal liquid (L) and gas (G). We require that the volume fraction of the colloidal liquid is sufficient to exhibit slow dynamics leading to a long-lived network. Hard spheres (without attraction $\varepsilon = 0$) do not form gels. Yellow shaded region indicates colloidal liquid-gas phase coexistence. Dashed line indicates a path for gelation.

massively increases the density difference between the isotropic and nematic phases.

This quantitative agreement with the theoretical phase behavior for hard rods suggests that attractions are not important, but residual attractions cannot be ruled out. However, significant attractions along the length of the rods cause *bundling* (29, 30), while "patchy" attractions lead to the formation of a random network of rods (30). While it is hard to be certain of the absence of attractions, since either bundling or a random network would suppress the isotropic–nematic transition, the occurrence of the transition suggests that for our system neither effect is dominant. We therefore conclude that any attractions are weak. This is quite different to conventional gelation in spheres, where attractions *drive* gelation (1, 14).

A further interesting observation concerns the shape of the nematic regions as shown in the confocal image in Fig. 2(a). Here the contrast is due to the much higher concentration of rods in the nematic compared to the isotropic phase, and the brightness levels are set such that isotropic appears dark. Nucleating nematic droplets are expected to be elongated in shape, approximately elliptical, but with sharp ends (*i.e.* tactoids) (31), as has been observed in experiments on more monodisperse systems than those we consider here (32, 33). Indeed the morphology of the bicontinuous network is consistent with tactoid-like objects having fused together. Thus we cannot rule out the formation of tactoids and their subsequent coalescence prior to imaging. Note also that since the rod width is sub-resolution, we do not obtain the local director field in our experimental data.

B. Spinodal decomposition. Allied with the observation of morphology distinct from that of (isolated) tactoids anticipated in the case of nucleation and growth, we find that the isotropic-nematic phase separation occurs in a spinodal-like fashion. Even at the shortest observation time accessible to our experiments (45 s from stopping vortex mixing) and at the weakest supersaturation (ϕ=0.021) we never observed nucleation and growth. That is to say, we did not find nucleation of nematic regions, these had always formed prior to our shortest observation time.

Gels often exhibit a bicontinuous texture. In Fig. 3(a) we show a 3d rendering of regions identified as nematic. We have confirmed that the regions identified as the nematic phase indeed percolate in all three dimensions and thus conclude that the percolation requirement for gelation is met. Close inspection of data such as that rendered in Fig. 3(a) suggests some alignment of the nematic domains. We believe this to be related to the capillary into which the sample is flowed for imaging. Such alignment may present an opportunity to produce networks whose orientation may be controlled.

C. Dynamics. We now turn to the dynamical asymmetry between the phases which is a necessary ingredient for viscoelastic phase separation, i.e. spinodal gelation (2). We shall see that our system exhibits a rather unusual form of dynamic asymmetry, due to the anisotropic dynamics of the nematic phase. In both our experiments and simulations, we measure the dynamics in a system of either isotropic or nematic phase. In this way, we probe the dynamics of the bulk phase, rather than domains in the gel network. To measure the dynamical behaviour in our experiments, we use a time correlation function $c(t)$, which measures the dynamics using *pixel intensities* (34). Because the width of the rods is sub-pixel resolution (a pixel corresponds to 240 nm), our analysis gives a coarse-grained measure of the dynamics rather than probing individual rods. In the nematic phase, where the particle separation is sub-resolution, a number of rods contribute to each pixel.

In Fig. 3(b) we fit the time correlation function according to a stretched exponential form $c(t) = c_0 \exp[-(t/\tau)^b]$, where c_0 and b are constants, to obtain a measure of the structural relaxation time. From our fitting, we determine relaxation times of $\tau_{\rm iso} = 270$ ms for the isotropic and $\tau_{\rm nem} = 202$ s for the nematic, thus indicating a considerable degree of dynamic asymmetry of three orders of magnitude. See Methods for further details. Our experimental data suggest that this dynamical asymmetry is comparable to the differences in dynamic properties of fast and slow phases in gels made of spheres (15).

Further insight is gained from simulation data shown in Fig. 3(c) which suggest that the situation is profoundly different to the case of spheres, in which the dynamics have no preferred direction. Here we compare the intermediate scattering function $F(k,t)$ (see SI) at global volume fractions $\phi = 0.012$ and $\phi = 0.36$, which correspond to the isotropic and nematic phase respectively. Note that, unlike in the experiments which consider a coarse-grained dynamics, here we consider the particle dynamics but at a similar lengthscale with respect to the rod dimensions. We see that the dynamics of the nematic phase is such that the relaxation time perpendicular to the director is around ten times longer than that along the director. At concentrations in the coexistence region, this leads to a long-lived network of flowing channels, promoting the lifetime of the network. The main result here is qualitative: in

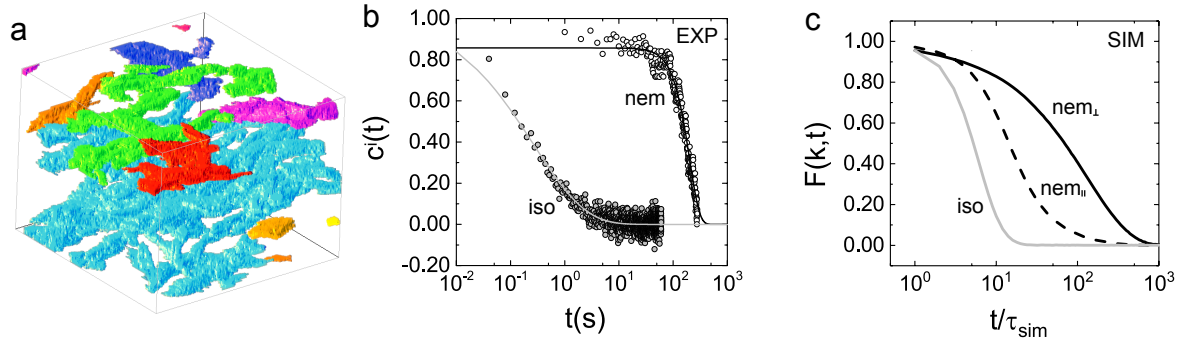

Fig. 3. Polydisperse hard rods exhibit the properties required for spinodal gelation: a percolating network and dynamic asymmetry. (a) 3d rendering of nematic domains identified from a confocal microscopy image of a sample with a bulk effective volume fraction $\phi = 0.043$ prior to phase separation. The image corresponds to $t = 993$s and shows a volume with dimensions of $58 \times 58 \times 35\ \mu m$. Colours denote connected domains. Blue domain percolates the 3d image. (b) Intensity time-correlation functions for the isotropic and nematic phases. The correlation function $c(t)$ is detailed in the main text, and shows that the nematic phase exhibits very much slower dynamics than does the isotropic. The lines are fits to a stretched exponential from which we extract the relaxation time for each phase. Note that here we consider a coarse-grained description of the particle dynamics, as discussed in the text. (c) Computer simulation data for intermediate scattering functions (which characterise particle motion). Here we distinguish the orientation in the case of the nematic between parallel and perpendicular to the director. The wavevector $k = 0.789$ is chosen to correspond to 240 nm, which is the pixel size in the experiments. The volume fractions are $\phi = 0.012$ and $\phi = 0.36$ for the isotropic and nematic data respectively.

both experiment and simulation, nematic and isotropic phases have strong dynamical contrast. Thus we argue that three key ingredients for gelation are present: spinodal decomposition leading to a bicontinuous (percolating) network of nematic and isotropic domains [criteria (*i*) and (*iii*)] and dynamical contrast between the two phases [criterion (*ii*)]. By analogy to work with spheres (14), within each phase, we expect the molecular dynamics to be a reasonable description of the real dynamics. Below, we consider the time-evolution (aging) of this non-equilibrium system, criterion (*iv*).

Not all volume fractions in the simulations map to those in the corresponding experiments. In particular we find the isotropic phase at somewhat higher volume fraction than in the experiments. We note that determining *effective* volume fractions in experiments is a challenging task (35), not to mention that the gels formed are of course out of equilibrium, so we would not necessarily expect a perfect mapping. We leave the accurate determination of the equilibrium phase diagram of this system to the future, noting that the network which forms is out of equilibrium, and that the experiments and simulations do follow different dynamics, which can influence the network formation (36).

D. Coarsening. A further key feature of gels formed by spinodal decomposition is that they coarsen over time, and this is governed by the dynamics of the more viscous phase (2, 15, 26). Our system is no exception and in Fig. 4 we present the coarsening behaviour at different volume fractions in the coexistence region (see Methods). The confocal images and 3d renderings in Figs. 4(a) and (b) reveal structural evolution of the nematic network for $\phi = 0.043$ at $t = 149$ and 993 s from the start of the experiment. To obtain a quantitative description of coarsening, we determine a lengthscale from the domain size. To do this we fit $h(r) = g(r) - 1$ with an exponential decay $h(r) = A\exp(-r/\xi)$ where A is a constant and ξ is a correlation length which measures the extent of the nematic domains. Here $g(r)$ is the pixel based radial distribution function (see SI). Note that we have imposed a spherically symmetric lengthscale on a system of anisotropic particles. The lengthscales resulting from fitting of $h(r)$ are shown in Fig. 4(d) for a range of rod volume fractions. At early times, for our deepest quench ($\phi = 0.066$), the initial growth rate has an exponent $> 1/2$ [solid line in Fig. 4(d)]. This is faster growth than for gels formed of spheres (15, 37), but at longer times and for weaker quenches, the growth rate is reduced and for certain values is compatible with that of diffusive growth of 1/3 [dashed line in Fig. 4(d)]. We carry out a similar analysis for the simulation data at $\phi = 0.140$, which is in the coexistence region [see Fig. 1(b))]. The correlation functions $h(r)$ here are based on the correlations of the rod centres, and fitted with exponentials to obtain a correlation length ξ. These lengths are plotted in Fig. 4(d) with the time scaled to the experiments by using the relaxation time in the isotropic phase τ_I to fix the timescale for both simulations and experiments. We see very similar time-evolution between the simulations and experiments. This is supportive of the idea that any residual attractions in the experimental system are unimportant, however our choice of dynamics in the simulations may affect the rate of coarsening. Overall, the clear observation of coarsening satisfies criterion *iv* for the time-evolution of gels.

3. Conclusion and discussion

We have argued that the properties of particulate gels, which have until now been associated with systems of *attractive* particles can in fact be realised with polydisperse colloidal rods without significant attractions. By conceptual arguments, based on the dynamical contrast between the isotropic and nematic phases and spinodal demixing, we have made the case that such gels may be found in systems of rods with sufficient polydispersity, with the novel feature that the viscosity of the nematic network is anisotropic: material can flow along the interior of the "arms" of the network.

This prediction we have realised using a colloidal model system of polydisperse rods of sepiolite clay. We have presented four key pieces of evidence in support of our claim, which we have supported with molecular dynamics simulations. Firstly, the system undergoes spinodal decomposition. Secondly, the phase coexistence in these polydisperse hard rods is broad enough that the density of the nematic phase (around 9 times higher than the coexisting isotropic phase) is sufficient that significant dynamic contrast between the phases is expected.

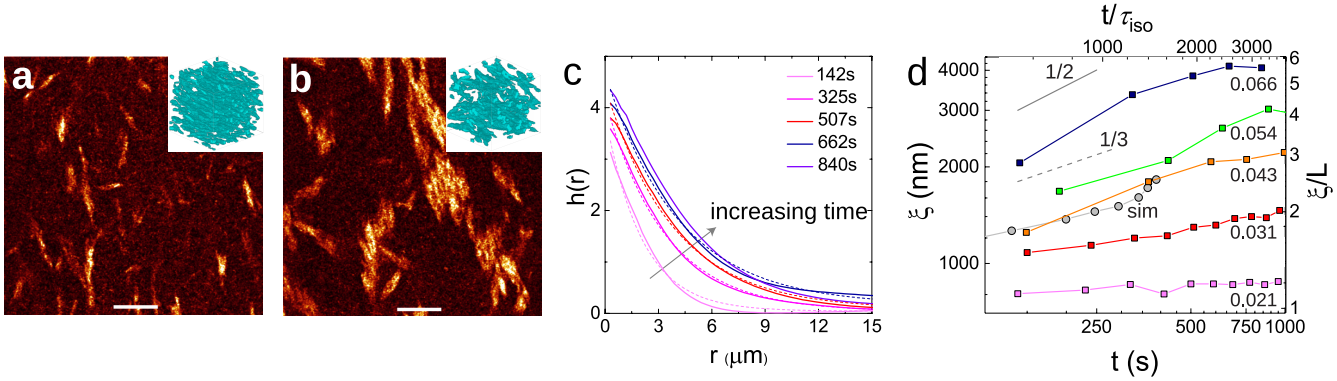

Fig. 4. Time-evolution of the system. Confocal images for a bulk volume fraction of, *i.e.* prior to demixing $\phi = 0.043$, at 149 s (a) and 993 s (b) showing coarsening of the network. Scale bars represent $10\ \mu$m. Insets in (a) and (b) correspond to 3d renderings of each sample where connectivity is clearly shown. The 3d volumes have dimensions $58 \times 58 \times 58\ \mu m$. Insets show renderings of the full 3d image. (c) Pair correlation functions $h(r)$ plotted at the times shown in seconds for $\phi = 0.066$ (thick solid lines). These are fitted with a decaying exponential (dashed lines) as described in the text. (d) Quantifying coarsening with the correlation length obtained from pair correlation $h(r)$ fitting. Grey solid line indicates an exponent of $1/2$, dashed line $1/3$ as indicated. Bulk rod volume fractions are indicated for the experimental data.

We determine the dynamic contrast, with the nematic phase being much more viscous than the isotropic phase in our experiments, while our simulation data reveals strong anisotropy in the dynamics of the nematic phase. In particular, we find that the rods can readily diffuse along the director, but exhibit significant dynamic slowing perpendicular to the director. Thirdly, we have shown that the nematic phase percolates. Finally, we find coarsening behaviour of the nematic domains, which is characteristic of domain coarsening in spinodal gels. We thus demonstrate a new class of *non-sticky* gels.

We note a novel feature of our system distinct from gels formed of spheres. In the case of spheres, as indicated in the phase diagram of Fig. 2(b), the density of the colloid-rich phase is a strong function of attraction strength and at high density the dynamics of spheres is a strong function of density (15). Thus, in addition to the effects of changing the interactions between the particles, the attraction strength provides a parameter by which the density of the colloid-rich network may be controlled. In particular, one finds that moving deeper in the gel region of the phase diagram upon increasing the attraction, that the rate of coarsening slows drastically, owing to the slower dynamics of the increasingly dense colloid-rich phase of spheres (2, 15).

In the case of our rods, the situation is profoundly different. In this athermal system, the rod volume fraction of the nematic phase at phase coexistence is fixed at $\phi_{\rm nem}^{\rm coex} = 0.215$. We see in Fig. 4 that, rather than slowing down upon moving deeper into the gel region by increasing ϕ (the global rod volume fraction), the rate of coarsening actually *accelerates*. We presume this is due either to the increased thermodynamic driving force for phase separation upon increasing volume fraction or to some coupling between the dynamic anisotropy of the nematic phase and the size of the domains. It would be very interesting to explore whether the same behaviour might occur in the case of spheres by moving horizontally across the gel region of the phase diagram in the (ε, ϕ) plane, as indicated by the dashed black line in Fig. 2(b), rather than vertically by changing the attraction strength ε as is usually done.

It is possible to add attraction between the particles to this system by adding polymers (29). Upon adding polymer, we expect a broadening of the isotropic-nematic phase coexistence (38). Under these conditions we expect that the gelation we observe here would be even more marked because the dynamic contrast between the phases would be even larger. This further leads to the question as to whether a *more* polydisperse system than those we have considered would in fact lead to a nematic phase with even slower dynamics than that we observe here.

A natural extension of this work is to enquire whether such behaviour is restricted to rod-like particles. We expect that this "non-sticky" gelation may be exhibited by a variety of anisotropic particles, which exhibit a phase coexistence gap such that the viscosity of the coexisting phases is sufficiently different. The dynamic anisotropy of course depends on the shape of the particles, but we expect that plate-like particles may exhibit comparable behaviour, if the coexistence gap between their isotropic and nematic phases is large enough. More generally, the phase behaviour of a large variety of anisotropic hard particles has recently been calculated (39, 40). Determination of coexistence gaps, and particularly dynamic contrast between their coexisting phases, likely in the case of polydispersity, may show that a wide range of particle shapes exhibit non-sticky gelation.

Materials and Methods

Sample preparation. Colloidal rod suspensions were made using sepiolite mineral clay particles. The zeolitic water was displaced by the fluorescent dye acridine orange (41). The dye-doped particles were treated with surfactant cetyltrimethylammonium bromide solution in deionized water and centrifuged. The clay particles were dispersed in toluene and stabilized using a polymer coating of SAP230 (Infineum, UK). Further details can be found in the SI.

Time correlation functions. The dynamics of the system were characterised using time sequences of xy images. The time resolved correlation (TRC) technique (34) was used in images at t' and $t'+t$ values, where t represents the time over which the correlation is made. This technique measures the change in configuration by calculating the degree of correlation in the images. This correlation is calculated using individual pixel intensity values $I(\mathbf{r}, t)$ of the images captured, and can be written as

$$C^i(t,t') = \frac{\langle I(\mathbf{r},t')I(\mathbf{r},t'+t)\rangle_{\rm pix}}{\langle I(\mathbf{r},t')\rangle_{\rm pix}\langle I(\mathbf{r},t'+t)\rangle_{\rm pix}} - 1. \qquad [1]$$

$\langle\rangle_{\rm pix}$ indicates average over all the pixels in the image. The correlation index $C^i(t,t')$ can be normalized as $c(t,t') = C^i(t,t')/C^i(0,t')$ to obtain a measurement of the relaxation time in each phase.

To obtain fully demixed isotropic and nematic phases, a suspension in the coexistence regime was allowed to phase separate in a capillary for 48 h. This compares to the timescale of the gel which is several hours. Each phase was imaged far from the interface and the walls of the capillary. Two different time steps τ were chosen: 0.020 s for the isotropic phase and 1.0 s for the nematic phase. The data in Fig. 3(b) has been corrected to account for noise in the intensity measured with the confocal microscope. This was made by normalizing the $c(t)$ values obtained with the first point in the correlation curve. To make the dynamic contrast clear, we subtract the constant value that $c(t \to \infty)$ approaches at long times, prior to the fitting in Fig. 3(b). The pixel size of the images used was close to 240 nm, around eight times the rod diameter. This sets the lengthscale over which the dynamics are probed in Fig. 3(b).

Computer simulations. We modelled our colloidal rods as linear rigid bodies composed of a number of spheres of mass m that interact only with the spheres of neighbouring rods via a Weeks-Chandler-Andersen potential,

$$u_{\mathrm{WCA}}(r) = \begin{cases} 4\epsilon\left[\left(\frac{\sigma}{r}\right)^{12} - \left(\frac{\sigma}{r}\right)^{6}\right] + \epsilon & r < 2^{1/6}\sigma, \\ 0 & r \geq 2^{1/6}\sigma, \end{cases} \quad [2]$$

where r is the center-of-mass distance between two spheres, σ is the approximated diameter of the repulsive core and ϵ is the strength of the interaction in units of k_BT. For simplicity we have set $\epsilon = 1$ and $\sigma = 1$, and the unit of time $\tau_{\mathrm{sim}} = \sqrt{m\sigma^2/k_BT}$. Two spheres were used for each rod segment of length 1σ, giving a total of 3,117,060 spheres for the small box of 65,000 rods and 8,632,884 spheres for the large box of 180,000 rods. The volume fractions were calculated by modelling the rods as hard spherocylinders with diameter $D = \sigma = 1$ to approximate the hard core.

For our simulations we used the open source MD simulation package LAMMPS (42), which has a dynamical integrator for rigid bodies (43, 44). To simulate our experimental conditions, we first equilibrated a system of polydisperse rods at a low volume fraction (ϕ<0.01) in a NVT ensemble using a Nóse-Hoover thermostat with chains (45). After this, an NPT ensemble with a Nóse-Hoover barostat and thermostat with chains was used to reach the desired concentrations. A final production run was carried out in an NVT ensemble. Two simulation time steps were used. For the sample preparation up to the desired volume fraction the time step was fixed to $\delta t = 0.001\ \tau_{\mathrm{sim}}$. The production run was carried out using $\delta t = 0.005\ \tau_{\mathrm{sim}}$. Total simulation times were of $2 \times 10^4\ \tau_{\mathrm{sim}}$ to $6 \times 10^4\ \tau_{\mathrm{sim}}$ depending on the box size and packing fraction. Periodic boundary conditions are applied. All data plotted in this work can be downloaded from https://data.bris.ac.uk/data/XXXX.

ACKNOWLEDGMENTS. We are grateful to Bob Evans and Hajime Tanaka for helpful discussions and Mike Allen and Jens Eggers for a critical reading of the manuscript. Francesco Turci is gratefully acknowledged for help with the dynamical analysis. Richard Stenner, Jacek Wasik and Azaima Razali are thanked for help with some experiments. CFC acknowledges CONACYT and the Mexican Government for a student scholarship. CPR acknowledges the Royal Society and European Research Council (ERC Consolidator Grant NANOPRS, project number 617266). EPSRC grant code EP/H022333/1 is acknowledged for provision of the confocal microscope used in this work. We thank M. Perez (Tolsa, Spain) for donating the sepiolite clay. TEM studies were carried out in the Chemistry Imaging Facility at UoB with equipment funded by UoB and EPSRC (EP/K035746/1 and EP/M028216/1). This work was carried out using the computational facilities of the Advanced Computing Research Centre, University of Bristol (http://www.bris.ac.uk/acrc/).

1. Zaccarelli E (2007) Colloidal gels: Equilibrium and non-equilibrium routes. *J. Phys.: Condens. Matter* 19:323101.
2. Tanaka H (2000) Viscoelastic phase separation. *J. Phys.: Condens. Matter* 12:R207.
3. Cardinaux F, Gibaud T, Stradner A, Schurtenberger P (2007) Interplay between spinodal decomposition and glass formation in proteins exhibiting short-range attractions. *Phys. Rev. Lett.* 99:118301.
4. Jabbari-Farouji S, Wegdam G, Bonn D (2007) Gels and glasses in a single system: Evidence for an intricate free-energy landscape of glassy materials. *Phys. Rev. Lett.* 99:065701.
5. Tanaka H (2013) Viscoelastic phase separation in soft matter and foods. *Faraday Discuss.* 167:9–76.
6. Helgeson ME, Moran SE, An HZ, Doyle PS (2012) Mesoporous organohydrogels from thermogelling photocrosslinkable nanoemulsions. *Nature Mater.* 11:344–352.
7. Rose S, et al. (2014) Nanoparticle solutions as adhesives for gels and biological tissues. *Nature* 505:382–385.
8. Ulrich S, et al. (2009) Cooling and aggregation in wet granulates. *Phys. Rev. Lett.* 102:148002.
9. Bouttes D, Gouillart E, Boller E, Dalmas D, Vandembroucq D (2014) Fragmentation and limits to dynamical scaling in viscous coarsening: An interrupted in situ x-ray tomographic study. *Phys. Rev. Lett.* 112:245701.
10. Baumer RE, Demkowicz MJ (2013) Glass transition by gelation in a phase separating binary alloy. *Phys. Rev. Lett.* 110:145502.
11. Poon WCK (2002) The physics of a model colloid-polymer mixture. *J. Phys: Condens. Matter* 14(33):R859–R880.
12. Zhang TH, Klok J, Tromp RH, Groenewold J, Kegel WK (2012) Non-equilibrium cluster states in colloids with competing interactions. *Soft Matter* 8:667.
13. Lu PJ, et al. (2008) Gelation of particles with short-range attraction. *Nature* 453:499–504.
14. Royall CP, Williams SR, Tanaka H (2018) Vitrification and gelation in sticky spheres. *J. Chem. Phys.* 148:044501.
15. Zhang I, Royall CP, Faers MA, Bartlett P (2013) Phase separation dynamics in colloid-polymer mixtures: the effect of interaction range. *Soft Matter* 9:2076–2084.
16. van Bruggen MPB, Dhont JKG, Lekkerkerker HNW (1999) Morphology and kinetics of the isotropic-nematic phase transition in dispersions of hard rods. *Macromolecules* 32:2256–2264.
17. Ni R, Belli S, van Roij R, Dijkstra M (2010) Glassy dynamics, spinodal fluctuations, and the kinetic limit of nucleation in suspensions of colloidal hard rods. *Phys. Rev. Lett.* 105:088302.
18. Lettinga MP, et al. (2006) Nematic-isotropic spinodal decomposition kinetics of rodlike viruses. *Phys. Rev. E* 73:011412.
19. Cates ME, Fuchs M, Kroy K, Poon WCK, Puertas AM (2004) Theory and simulation of gelation, arrest and yielding in attracting colloids. *J. Phys.: Condens. Matter* 16:S4861.
20. Woolston P, van Duijneveldt JS (2015) Isotropic-nematic phase transition of polydisperse clay rods. *J. Chem. Phys.* 142:184901.
21. Speranza A, Sollich P (2002) Simplified Onsager theory for isotropic-nematic phase equilibria of length polydisperse hard rods. *J. Chem. Phys.* 117:5421–5436.
22. Lettinga MP, Dhont JKG, Zhang Z, Messlinger S, Gompper G (2010) Hydrodynamic interactions in rod suspensions with orientational ordering. *Soft Matter* 6:4556—-4562.
23. Onsager L (1949) The effects of shape on the interaction of colloidal particles. *Ann. N. Y. Acad. Sci.* 51:627–659.
24. Allen MP (1990) Diffusion coefficient increases with density in hard ellipsoid liquid crystals. *Phys. Rev. Lett.* 65:2881–2884.
25. van Bruggen MPB, Lekkerkerker HNW, Maret G, Dhont JKG (1998) Long-time translational self-diffusion in isotropic and nematic dispersions of colloidal rods. *Phys. Rev. E* 58:7668–7677.
26. Testard V, Bethier L, Kob W (2014) Intermittent dynamics and logarithmic domain growth during the spinodal decomposition of a glass-forming liquid. *J. Chem. Phys.* 140:164502.
27. Wensink HH, Vroege GJ (2003) Isotropic-nematic phase behavior of length-polydisperse hard rods. *J. Chem. Phys.* 119:6868–6882.
28. Bolhuis P, Frenkel D (1997) Tracing the phase boundaries of hard spherocylinders. *J. Chem. Phys.* 106:666–687.
29. Wilkins GMH, Spicer PT, Solomon MJ (2009) Colloidal system to explore structural and dynamical transitions in rod networks, gels, and glasses. *Langmuir* 25:8951–8959.
30. Kazem N, Carmel M, Maloney CE (2015) Gelation and mechanical response of patchy rods. *Soft Matter* 11:7877–7887.
31. Prinsen P, van der Schoot P (2003) Shape and director-field transformation of tactoids. *Phys. Rev. E* 68:021701.
32. Oakes PW, Viamontes J, Tang JX (2007) Growth of tactoidal droplets during the first-order isotropic to nematic phase transition of f-actin. *Phys. Rev. E* 75:061902.
33. Puech N, Grelet E, Poulin P, Blanc C, van der Schoot P (2010) Nematic droplets in aqueous dispersions of carbon nanotubes. *Phys. Rev. E* 82:020702.
34. Buzzaccaro S, Alaimo MD, Secchi E, Piazza R (2015) Spatially: resolved heterogeneous dynamics in a strong colloidal gel. *J. Phys.: Condens. Matter* 27(19):194120.
35. Royall CP, Poon WCK, Weeks ER (2013) In search of colloidal hard spheres. *Soft Matter* 9:17–27.
36. Royall CP, Eggers J, Furukawa A, Tanaka H (2015) Probing colloidal gels at multiple length scales: The role of hydrodynamics. *Phys. Rev. Lett.* 114:258302.
37. Testard V, Berthier L, Kob W (2011) Influence of the glass transition on the liquid-gas spinodal decomposition. *Phys. Rev. Lett.* 106:125702.
38. Tuinier R, Taniguchi T, Wensink H (2007) Phase behavior of a suspension of hard spherocylinders plus ideal polymer chains. *Eur. Phys. J. E.* 23:355–365.
39. Damasceno PF, Engel M, Glotzer SC (2012) Predictive self-assembly of polyhedra into complex structures. *Science* 337:453–457.
40. Dijkstra M (2014) Entropy-driven phase transitions in colloids: from spheres to anisotropic particles. *Adv. Chem. Phys.* 156:35–71.
41. Yasarawan N, van Duijneveldt JS (2010) Arrested phase separation of colloidal rod-sphere mixtures. *Soft Matter* 6(2):353–362.
42. Plimpton S (1995) Fast parallel algorithms for short-range molecular dynamics. *J. Comp. Phys.* 117(1):1–19.
43. Miller TF, et al. (2002) Symplectic quaternion scheme for biophysical molecular dynamics. *J. Chem. Phys.* 116(20):8649–8659.
44. Kamberaj H, Low R, Neal M (2005) Time reversible and symplectic integrators for molecular dynamics simulations of rigid molecules. *The Journal of chemical physics* 122(22):224114.
45. Martyna GJ, Klein ML, Tuckerman M (1992) Nosé–Hoover chains: the canonical ensemble via continuous dynamics. *J. Chem. Phys.* 97:2635–2643.